

Received 21 November 2023, accepted 27 November 2023, date of publication 8 December 2023,  
date of current version 14 December 2023.

Digital Object Identifier 10.1109/ACCESS.2023.3341102

## RESEARCH ARTICLE

# Pre Synchronization Control Strategy of Virtual Synchronous Generator (VSG) in Micro-Grid

JIANFENG WANG<sup>1,2</sup>, NURULAZLINA RAMLI<sup>1</sup>, (Member, IEEE),  
AND NOOR HAFIZAH ABDUL AZIZ<sup>3</sup>

<sup>1</sup>Centre of Advanced Electrical and Electronic Systems (CAEES), Faculty of Engineering and the Built Environment, SEGi University, Petaling Jaya, Selangor 47810, Malaysia

<sup>2</sup>Faculty of Electrical Engineering, Hebei Vocational University of Technology and Engineering, Xingtai 054000, China

<sup>3</sup>School of Electrical Engineering, College of Engineering, Universiti Teknologi MARA (UiTM), Shah Alam, Selangor 40450, Malaysia

Corresponding author: Jianfeng Wang (ncepu\_wjf@163.com)

This work was supported by the Fundamental Research Funds for the Central Universities under Grant 2021MS123.


**ABSTRACT** The constant increase of energy demand and the widespread adoption of renewable energy sources have led to the significant interest in micro-grids, which are small-scale power systems that utilize distributed energy resources. However, micro-grids face synchronization challenges in terms of stability and reliability, and virtual synchronous generator technology has become the key to addressing this issue. This study focuses on the pre synchronization control strategy of virtual synchronous generators in micro-grids, aiming to solve the potential surge current problem that virtual synchronous generators may generate when switching from off grid mode to grid connected mode through innovative methods. This strategy employs a phase difference acquisition method that eliminates the need for a phase-locked loop. It calculates virtual power by utilizing the output voltage of the virtual synchronous generator and the grid side voltage, and obtains the phase difference through calculation. The resulting phase difference is then used as input for the frequency phase synchronization unit in pre-synchronization. By adjusting the diagonal frequency, the phase difference  $\Delta\theta$  can be modified to achieve pre-synchronization before connecting the virtual synchronous generator to the power grid. This method notably reduces the dependence on the phase-locked loop and enhances the stability and reliability of the system. The paper has effectively solved the synchronization problem of virtual synchronous generators in micro-grids through innovative pre synchronization control strategies and improved secondary frequency regulation strategies. It is hoped that these research results will provide new ideas and methods for the further development and application of micro-grid technology.

**INDEX TERMS** VSG, pre-synchronization control strategy, micro-grid, phase angle difference acquisition method, operational stability, performance enhancement, grid connection process, output frequency adjustment, phase difference, high-precision pre-synchronization, reliability and response speed.

## I. INTRODUCTION

### A. MOTIVATION AND INCENTIVES

With the continuous growth of global energy demand and the rapid development of renewable energy, micro-grids, as a flexible energy distribution and management method, have become an effective way to solve important issues such as energy supply security and environmental sustainability [1]. The construction and operation of micro-grids

The associate editor coordinating the review of this manuscript and approving it for publication was Qiang Li .

entail integrating and managing a variety of energy resources, such as solar energy, wind energy, energy storage systems, and conventional electric generators, with an aim to achieve optimal efficiency. In micro-grids, ensuring the coordinated operation and reliability of various energy resources is a challenging task. Virtual Synchronous Generator (VSG), as an emerging control strategy, has been widely researched and applied [2]. VSG simulates the dynamic characteristics of traditional synchronous generators and can provide the inertial support and frequency response required by the micro-grid system, thus improving the stability and robustness of the

micro-grid. However, in practical applications, there are still a series of problems and challenges in the pre-synchronization control strategy of VSG. How to better realize the coordinated operation of VSG and improve the performance and reliability of micro-grid still requires in-depth research and exploration [3]. Therefore, further research and exploration are needed to overcome these challenges, drive the development of micro-grids and virtual synchronous generator (VSG) technologies, and provide society with more sustainable and reliable energy solutions. This serves as the motivation for research and innovation in this field, as addressing these issues will have a significant impact on the future energy systems of society.

## B. LITERATURE REVIEW

The VSG pre-synchronization control strategy plays a key role in the micro-grid system and helps to improve the stability and reliability of the system. Many experts have studied it. To eliminate the need for phase-locked loop (PLL) and islanding detection technology during mode conversion, Srinivas V L and other scholars proposed a control strategy to achieve seamless transition of three-phase VSGs based on inverter current and voltage sensor data. At the same time, it automatically adapted to mode conversion. The mathematical formula for the controller was established and the closed-loop stability of the system was evaluated using the eigenvalue stability analysis method. The results showed that this approach eliminated the need for PLLs and islanding detection techniques, as well as multiple feedback loops and complex adjustments to proportional-integral regulators [4]. To address how Inverter-based micro-grids (IMGs) maintain stability during various operational modes to support power sharing and voltage/frequency regulation in overloaded micro-grids, Naderi et al. conducted a comprehensive review of IMG concepts, models, and stability analyses. Additionally, they extensively researched control methods literature from multiple perspectives. Concept maps, classification tables, and support for offline and real-time simulation using MATLAB and OPAL-RT simulators were provided for comparative analysis [5]. Aiming at the problem of how to establish a small-signal dynamic model to design the inertia and damping of VSG according to the capacity ratio of VSG and SG units, thereby improving the transient performance of the micro-grid system, Shi et al. designed and proposed a novel prediction method. Synchronous control method was used to solve the transient performance problem of VSG and SG in micro-grid. A small-signal dynamic model was established, allowing the inertia and damping parameters of the VSG to be optimized based on the capacity ratio of the VSG and SG units. The proposed novel pre-synchronization control method successfully eliminated the phase jump between VSG and SG while meeting the requirement of generator unit shutdown or re-shutdown, thereby improving the transient performance of the micro-grid system [6]. Liu et al. developed a pre-synchronization control strategy to address

the challenge of designing a strategy for fast and dependable power grid connection. Their approach employed periodic pulses with a specified duty cycle to enable the inverter to operate with unity power factor in rectifier mode, facilitating grid synchronization. A synchronous reference frame PLL was used to obtain the current phase, and the initial phase of the AC grid was estimated by sampling the current to achieve reliable grid connection. The proposed pre-synchronization control strategy successfully solves the problem that sensorless control easily leads to an increase in surge current and achieves reliable grid connection [7].

In summary, although many experts have conducted in-depth research on VSG pre-synchronization control strategies, there is still some room for improvement in terms of system-level integration and coordination. The paper aims to fill this gap and proposes a new pre-synchronization control strategy that simplifies the system under fuzzy control and designs the secondary frequency modulation parameters. The main contribution of the paper is that the method proposed in the study not only makes the system simpler, but also is expected to improve the performance of micro-grids and distributed energy systems by designing secondary frequency modulation parameters. This will help drive the development of clean energy and enable a more sustainable and reliable energy supply.

## C. CONTRIBUTION AND PAPER ORGANIZATION

The innovation of the research is that through in-depth research on the VSG pre-synchronization control strategy, it provides important support for the sustainable development of the micro-grid system. By optimizing the design and control strategy of VSG, renewable energy resources can be better integrated, the robustness of micro-grids can be improved, and dependence on traditional power generators can be reduced, thus promoting the wider application of clean energy. This will help meet future energy needs, reduce dependence on fossil fuels, reduce environmental impact and promote sustainable development. The research is divided into four parts. The first part is a summary of VSG pre-synchronization control strategy and micro-grid research. The second part is the research on designing VSG pre-synchronization control strategy, from off-grid to grid-connected control strategy, and secondary frequency modulation method. The third part is the verification of the VSG pre-synchronization control strategy, and the fourth part is the summary of the entire text.

## II. DESIGN OF VSG PRE-SYNCHRONIZATION CONTROL STRATEGY

The active frequency control and reactive voltage control stages of the VSG control strategy are key parts in achieving the matching between VSG and the power grid [8]. These two connections are utilized to regulate the VSG's output power and frequency, as well as its reactive power and voltage. This ensures that the VSG's active power, frequency, and reactive power and voltage are aligned with the grid prior to

its connection. The active frequency control link is mainly used to control the output power and frequency of the VSG to match with the active power and frequency of the power grid [9]. This control link adjusts the output frequency of VSG to keep it consistent with the frequency of the power grid based on the frequency changes. The fundamental concept involves determining the frequency error by measuring the variance between the grid frequency and the VSG output frequency. Subsequently, the output power of the VSG is regulated based on the error's magnitude. By combining the governor equation of the prime mover and the rotor equation of motion of the synchronous generator, the active frequency control link of the VSG control strategy can be obtained [10]. According to the characteristics of the prime mover governor, the mechanical power output by the prime mover can be expressed as shown in equation 1.

$$P_m = P_{ref} + K_\omega(\omega_0 - \omega) \quad (1)$$

In equation (1),  $P_m$  represents the power generated by the rotating device provided by the prime mover.  $P_{ref}$  is the set expected power level used to control the target power output in the system.  $K_\omega$  represents the relationship between the output power of the prime mover and the grid frequency, specifically the degree of change in the output power of the prime mover when the system frequency decreases.  $\omega_0$  represents the calibrated angular velocity, and  $\omega$  represents the actual angular velocity. The formula of the synchronous generator rotor motion behavior is shown in equation (2).

$$\begin{cases} \omega - \omega_g = \frac{d\delta}{dt} \\ J \frac{d(\omega - \omega_g)}{dt} = T_m - T_e - D(\omega - \omega_g) \end{cases} \quad (2)$$

In equation (2), the system frequency of grid  $\omega_g$  and  $\delta$  represents the phase angle.  $J$  is the moment of inertia, and  $T_m$  is the output torque of the prime mover.  $T_e$  is the generator torque output by the generator, and  $D$  is the damping constant of the rotor [11]. The power relationship between the output torque of the prime mover and the generator torque output is shown in equation (3).

$$\begin{cases} T_e = \frac{P_e}{\omega} \approx \frac{P_e}{\omega_0} \\ T_m = \frac{P_m}{\omega} \approx \frac{P_m}{\omega_0} \end{cases} \quad (3)$$

In equation (3),  $P_e$  represents the generator torque output by the synchronous generator. Due to the fact that in actual operation, the power grid usually operates at a frequency close to the rated frequency  $\omega$ , then the numerical work can be obtained,  $\omega_g \approx \omega_0$ . The expression of equations of motion of generator rotor after synchronization is shown in equation (4).

$$\begin{cases} \frac{P_m}{\omega_0} - \frac{P_e}{\omega_0} - D(\omega - \omega_g) = J \frac{d(\omega - \omega_0)}{dt} \\ \omega - \omega_0 = \frac{d\delta}{dt} \end{cases} \quad (4)$$

By combining equations (1) and (4), the control equation of the active frequency link in the VSG control strategy can be obtained. In this control equation, the active output power  $P_e$  is usually taken as the output power  $P_{out}$  of VSG. Therefore, the control equation of the active frequency link of VSG can be expressed as equation (5).

$$\begin{cases} \frac{P_{ref} + K_\omega(\omega - \omega_g) - P_{out}}{\omega_0} - D(\omega - \omega_g) = J \frac{d(\omega - \omega_0)}{dt} \\ \omega - \omega_0 = \frac{d\delta}{dt} \end{cases} \quad (5)$$

By controlling the equation, the reactive power output of VSG can be adjusted. This control strategy can achieve reactive voltage control of VSG in the micro-grid and ensure voltage consistency between the micro-grid and the power grid [12]. By controlling the reactive power voltage link, the reactive power in the micro-grid can be effectively managed and the voltage stability of the micro-grid can be controlled. The expression for the reactive voltage link is shown in equation (6).

$$U_{ref} = U_0 + K_u(Q_{ref} - Q_{out}) \quad (6)$$

In equation (6),  $U_{ref}$  represents the reference voltage output amplitude.  $U_0$  is the rated voltage amplitude.  $K_u$  represents the reactive power voltage drop coefficient.  $Q_{ref}$  represents the specified reactive power.  $Q_{out}$  is the actual reactive power output of VSG. In grid-connected mode, VSG simulates the primary voltage regulation characteristics of synchronous generators through equation (6) and can participate in reactive voltage regulation of the power grid. In off-grid mode, VSG adjusts the amplitude of its output voltage based on the output reactive power [13]. This control strategy enables VSG to simulate the voltage regulation characteristics of synchronous generators, flexibly adjusting reactive power and voltage amplitude in various operating modes to attain stable operation and power balance control within micro-grid systems.

According to Figure 1, the active frequency link obtains the phase information  $\theta$  of the reference voltage through the corresponding calculation method. The reactive voltage link, on the other hand, undergoes corresponding calculations to obtain the amplitude information  $U_{ref}$  of the reference voltage. The two parameters  $U_{ref}$  and  $\theta$  are combined to form the reference three-phase voltage  $U_{ref} \angle \theta$ , and then through the double closed-loop control of voltage and current, the control waveform used to modulate the inverter switch is generated. This process achieves the control of the VSG, ensuring that its output voltage and frequency match the power grid, thereby solving the synchronization problem in the micro-grid and improving the stability and reliability of the system.

### III. VSG CONTROL STRATEGY FROM OFF GRID TO GRID CONNECTION

To obtain the information of phase difference  $\Delta\theta$  more conveniently, a method is proposed to obtain phase difference

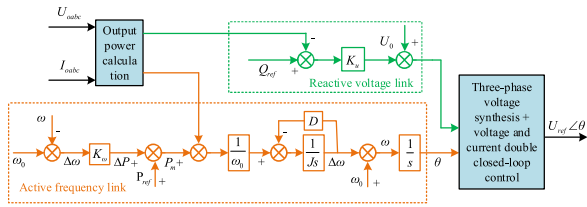


FIGURE 1. Overall control block diagram of VSG control strategy.

$\Delta\theta$  without using a PLL to obtain phase angle information. Firstly, the output voltage  $U_o \angle \theta_o$  of VSG and the voltage  $U_o \angle \theta_g$  on the grid side are obtained, and then the two voltage signals are transmitted to the control unit. In the control unit, phase difference information can be derived through calculations. As shown in equation (7).

$$\begin{cases} P_v = \frac{3(U_o^2 - U_o U_g \cos \Delta\theta)}{R_v} \\ Q_v = \frac{-U_o U_g \sin \Delta\theta}{R_v} \end{cases} \quad (7)$$

In formula (7),  $P_v$  is the active power,  $Q_v$  is the reactive power,  $U_o$  is the effective value of the VSG output voltage, and  $U_g$  is the effective value of the grid side voltage. The method for phase difference acquisition without the use of a PLL includes the following steps. First, the current in the sampling system is acquired, and the phase of the voltage is measured. Subsequently, phase information is obtained by calculating the phase difference between the current and voltage, which can be computed using trigonometric functions such as sine and cosine. Once the phase difference information is obtained, it can be applied to the control system operation. Finally, the system needs to be calibrated and optimized to ensure accuracy and stability [14]. As shown in equation (8).

$$\Delta\theta = \arccos\left(\frac{U_o^2 - \frac{P_v \cdot R_v}{3}}{U_o U_g}\right) \quad (8)$$

In equation (8),  $P_v$  is the virtual active power and  $R_v$  is the assumed virtual line resistance.  $U_o$  and  $U_g$  represent the effective value of VSG output voltage and the effective value of grid side voltage, respectively. The value of  $\Delta\theta$  in VSG can be obtained through equation (8), as shown in Figure 2.

From Figure 2, the proposed secondary frequency control scheme based on VSG offers unique advantages and novelty compared to traditional approaches. Firstly, this scheme preserves the essential structure of VSG control without modifications to the mechanical equations, making the system's theory more explicit and stable. This contributes to maintaining the fundamental characteristics and performance of the VSG system. Secondly, the scheme closely follows the secondary frequency control process of the power system. In contrast to traditional methods, it only activates secondary frequency control when the system frequency exhibits significant deviations. During periods of load stability, the PI controller remains inactive to ensure the system's dynamic performance is optimal. Phase difference information can

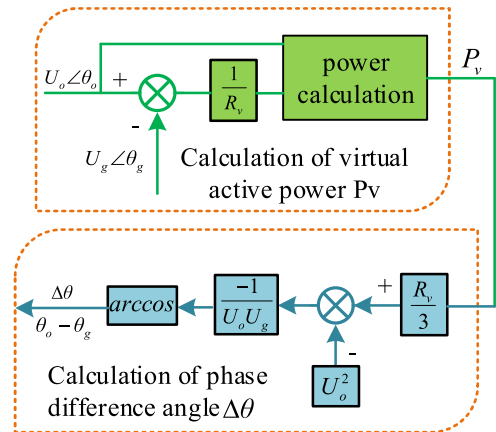


FIGURE 2. Schematic diagram of obtaining phase angle difference information by virtual active power.

be obtained without the use of PLL. This method includes two steps: calculating virtual active power  $P_v$  and calculating phase difference  $\Delta\theta$ . Firstly, the VSG output voltage and grid side voltage are collected, and then the virtual active power is calculated and relevant intermediate calculations are performed to obtain the phase difference  $\Delta\theta = \theta_o - \theta_g$  between the VSG output voltage and the grid side voltage. Next,  $\Delta\theta$  is input to the PI controller, and the Angular frequency compensation is added to the output frequency of the VSG power loop to adjust the phase angle and frequency. This method simplifies the process of obtaining phase difference information, avoids the use of traditional PLL, and can accurately control the phase and frequency of VSG output voltage. When the micro-grid operates in off-grid mode, VSG adjusts the output voltage and frequency through internal control strategies to meet the needs of off-grid loads. At this point, VSG operates independently and is not connected to the power grid, maintaining stable operation of the micro-grid [15]. When switching the micro-grid to grid connection mode, VSG needs to perform corresponding operations to ensure a smooth transition. Gradually increasing the output voltage and frequency of the VSG, and matching it with the voltage and frequency of the power grid while adjusting the phase to maintain VSG synchronization with the power grid can prevent excessive impact on the power grid and allow for a seamless connection [16]. Once VSG successfully switches to grid-connected mode and synchronizes with the grid, it will start operating in grid-connected mode. In grid connection mode, VSG will adjust based on the voltage, frequency, and phase of the grid to maintain stable connection between the micro-grid and the grid, and provide the required active and reactive power [17]. The control flow diagram of VSG pre synchronization process is Figure 3.

In Figure 3,  $S_g$  represents the grid-connected switch signal. When the micro-grid is in off-grid operation, the value of  $S_g$  is 0. When the micro-grid needs to switch to grid connection mode, the value of  $S_g$  becomes 1. In addition,  $S_p$  represents the frequency phase angle synchronization signal [7]. The pre



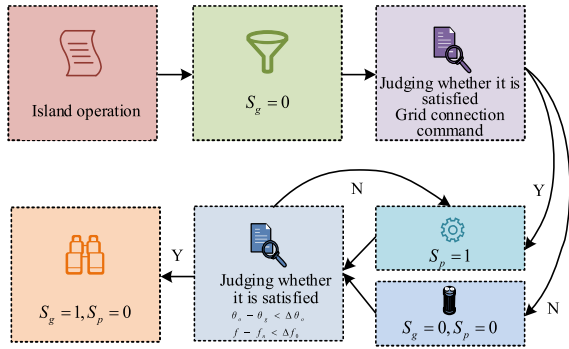


FIGURE 3. Control flow diagram of the VSG pre-synchronization process.

synchronization process is analyzed in combination with the Control-flow diagram in Figure 2. When the micro-grid is in off-grid operation,  $S_g$  is 0. After receiving the grid connection command at a certain moment, start the frequency phase angle synchronization link, that is, set  $S_p$  to 1, to achieve frequency and phase angle synchronization [18]. After the frequency and phase angle gradually synchronize to the allowable operating range, the pre synchronization process ends. At this point, turning off the frequency and phase synchronization signal, starting the grid connection switch, and the micro-grid successfully switches to grid connection mode.

**IV. SECONDARY FREQUENCY MODULATION TECHNOLOGY OF GENERATORS BASED ON VSG PRE SYNCHRONIZATION CONTROL**

Usually, generators need to operate within a certain frequency range, which may lead to instability of the power system or equipment damage. Thus, the inclusion of an integration link for frequency deviation enables the implementation of the conventional secondary frequency regulation strategy for the generator. This allows automatic adjustment of the output power based on the frequency deviation to maintain the frequency within a safe range. This control strategy helps to maintain the stable operation of the power system. To restore the power output of the generator to a safe operating range, an integration link for frequency deviation is incorporated into the active power control loop. This integration link accumulates the frequency deviation value based on time and allows for adjustments in frequency when exceeding the safe operating range [19]. As shown in equation (9).

$$\begin{cases} P_{ref} + K\omega(\omega_0 - \omega) - P_{out} - D\omega_0(\omega - \omega_0) + \\ K_i \int (\omega - \omega_0)dt = J\omega_0 \frac{d(\omega - \omega_0)}{dt} \\ \frac{d\delta}{dt} = \omega - \omega_0 \end{cases} \quad (9)$$

In equation (9),  $K_i$  represents the parameter used in frequency recovery control to adjust the intensity of the frequency deviation integration link. In the conventional VSG secondary frequency modulation strategy, the control block diagram usually includes a frequency measurement module,

a frequency deviation calculation module, an integration link, a controller output module, and a generator power control module. According to equation (9), the control block diagram can adjust the output active power of the generator based on frequency deviation to achieve frequency recovery and stable operation [20]. Figure 4 is a block diagram of conventional VSG secondary frequency modulation control.

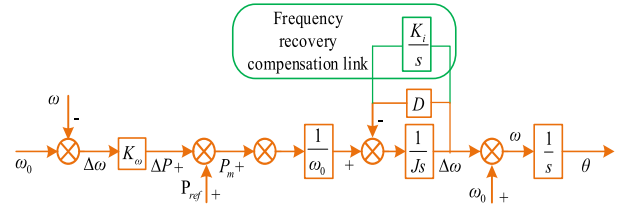


FIGURE 4. Conventional VSG secondary frequency modulation control block diagram.

The conventional VSG secondary frequency modulation strategy is a control method used to stabilize the frequency of power systems. In this strategy, the control system compensates by integrating the deviation of diagonal frequency, thereby adjusting the output frequency  $\omega$  of VSG to the rated frequency  $\omega_0$ .

$$\frac{\Delta\omega}{\Delta P_{out}} = -\frac{\frac{1}{J\omega_0}s}{s^2 + \left(\frac{D\omega_0 + K_\omega}{J\omega_0}\right)s + \frac{K_i}{J}} \quad (10)$$

To obtain the steady-state value of angular frequency  $\omega$ , the Laplace transform terminal value theorem is studied, which is used to solve the system’s response at steady-state, i.e. the value at  $t \rightarrow \infty$ , as shown in equation (11).

$$\lim_{t \rightarrow \infty} \Delta\omega = -\lim_{s \rightarrow 0} s \cdot \frac{\Delta P_{out}}{s} - \frac{\frac{1}{J\omega_0}s}{s^2 + \left(\frac{D\omega_0 + K_\omega}{J\omega_0}\right)s + \frac{K_i}{J}} = 0 \quad (11)$$

After adding the frequency recovery compensation link, the output frequency of VSG will eventually recover to the rated value after experiencing frequency changes caused by sudden load changes, that is, the steady-state value is 0 [21]. The frequency recovery process is a typical second-order system with natural oscillation angle frequency  $\omega_0$  and damping ratio  $\xi$ , which determines the speed and oscillation characteristics of frequency recovery [22]. The expression of natural oscillation angular frequency is equation (12).

$$\omega_n = \sqrt{\frac{K_i}{J}} \quad (12)$$

As equation (12), the natural oscillation angular frequency refers to the angular frequency of frequency deviation oscillation during the frequency recovery process. A larger  $\omega_0$  indicates a faster frequency recovery speed, while a smaller  $\omega_0$  indicates a slower frequency recovery. The damping ratio

expression is equation (13).

$$\xi = \frac{D\omega_0 + K_\omega}{2\omega_0\sqrt{K_i J}} \quad (13)$$

Damping ratio refers to the degree of attenuation of oscillation during the frequency recovery process, which reflects the stability of the frequency recovery process. The larger the damping ratio, the more stable the frequency recovery process will be, and excessive oscillation will not occur. A larger value  $\xi$  indicates a faster attenuation of the frequency recovery process, while a smaller value  $\xi$  indicates that there may be a prolonged oscillation, and the values of  $K_i$  and  $\xi$  are inversely proportional [23]. The paper proposes a VSG secondary frequency modulation strategy control method based on variable integral coefficient improvement, as shown in Figure 5.

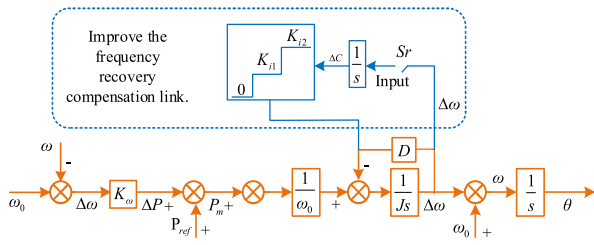


**FIGURE 5.** The control block diagram of the improved quadratic frequency modulation strategy with variable integral coefficient.

As Figure 5,  $S_r$  is used to control whether to activate the secondary frequency modulation strategy. When  $S_r = 0$ , it indicates that the secondary frequency modulation strategy will not be activated. When  $S_r = 1$  is set, it indicates the activation of the secondary frequency modulation strategy [24].  $\Delta C$  is used to compensate for frequency deviation, and its calculation formula is  $\Delta C = (\omega - \omega_0) / s$ , where  $\omega$  represents the actual frequency and  $s$  represents the time. After the secondary frequency modulation strategy is activated, the  $\Delta C$  information is fed into the integrator: once the secondary frequency modulation strategy is activated, the collected frequency deviation  $\Delta C$  will be fed into the integrator for integration calculation. To configure different integration coefficients  $K_{i1}$  and  $K_{i2}$  according to stages 1 and 2 of the frequency recovery process. Phase 1 adopts a larger integration coefficient  $K_{i1}$  to accelerate the frequency recovery process. In Phase 2, a smaller integration coefficient  $K_{i2}$  is used to ensure the stability of the frequency recovery process [25].

In the frequency recovery process, the first is to determine whether  $|\Delta C|$  is equal to 0 to determine whether there is additional active power caused by secondary frequency modulation. Then, based on the load size and frequency changes, the size of  $|\Delta P|$  and  $|\Delta P_0|$ , and whether the secondary frequency modulation control strategy needs to be activated are determined. If  $|\Delta P| < |\Delta P_0|$ , the secondary frequency modulation will not be activated, and  $K_i = 0$  and VSG will operate in the conventional primary frequency modulation mode. If  $|\Delta P| > |\Delta P_0|$  and  $|\Delta P| > 0$ , activate the secondary frequency control strategy.  $S_r = 1$ , configure different

integration coefficients  $K_i$  and  $K_{i1}$ . If  $|\Delta P| > |\Delta P_0|$  and  $|\Delta P| < 0$ , activate the frequency recovery control strategy.  $S_r = 1$ , configure different integration coefficients  $K_i$  and  $K_{i1}$ . If  $|\Delta C|$  is not equal to 0, a secondary frequency modulation is required,  $S_r = 1$ . In the case of load fluctuations, the size of  $\Delta P$  is determined to ensure the sudden increase or decrease in load, and configure the corresponding integration coefficient  $K_i$  to ensure the stable operation of the power system [26]. Next,  $\Delta P_0$  is designed to ensure that the output voltage and frequency of the VSG are not affected by external power systems during off grid operation. Therefore, the steady-state voltage and frequency will depend on the mechanical characteristics and load conditions of the VSG. As shown in equation (14).

$$\omega = \omega_0 - m_{VSG} (P_{out} - P_{ref}) \quad (14)$$

In equation (14), the equivalent sag relationship of VSG under steady-state conditions can be expressed as a sag coefficient, usually expressed as a percentage. The droop coefficient represents the degree to which the VSG output frequency changes relative to the load when the load changes. Specifically, when the droop coefficient is positive, the output frequency of VSG decreases with increasing load. When the droop coefficient is negative, the output frequency of VSG increases with increasing load. When the droop coefficient is zero, the output frequency of VSG remains constant, independent of load changes. As shown in equation (15).

$$\frac{|m_{VSG} (P_{out} - P_{ref})|}{2\pi} = 0.2\text{Hz} \quad (15)$$

In equation (15), according to national standards, the frequency of the power system should be controlled within the range of  $(50 \pm 0.2)$  Hz to maintain the stability and frequency control of the power system [27]. Therefore, in the study, it is also  $(50 \pm 0.2)$  Hz. During off-grid operation, VSG needs to adjust its output frequency based on load conditions and frequency changes to maintain it within the specified range, thereby ensuring the normal operation of the power system and power supply quality. Organizing equation (14) to obtain equation (16).

$$\Delta P_0 = |P_{out} - P_{ref}| < \frac{0.2}{m_{VSG}} = \frac{2\pi}{5} \cdot (D\omega_0 + K_\omega) \quad (16)$$

The final calculation yields  $\Delta P_0 = 3230$ . To design two more integration coefficients, where  $K_{i1}$  is the integration coefficient used for frequency recovery stage 1. In this stage 1, the system may have significant frequency deviation. Therefore, the value of  $K_{i1}$  should be between 0.1 and 0.3 for the typical second-order system damping ratio corresponding to frequency recovery stage 2 to ensure the speed and stability of frequency recovery. The study selects  $K_{i1} = 3000$  as the numerical value of the integration coefficient.  $K_p$  is the integration coefficient used for frequency recovery stage 2. In the stage 2, the response characteristics of the system are similar to those of a typical second-order system. The integral coefficient corresponding to the damping ratio  $\xi = 0.707$  of

the typical second-order system can be taken as the value of  $K_p$ . This can ensure stable system response in frequency recovery stage 2 and avoid excessive frequency deviation [28]. The specific expression is equation (17).

$$K_{i2} = \frac{(D\omega_0 + K\omega)}{2J\omega_0^2} \tag{17}$$

After calculation, the final value of equation (17) is  $K_{i2} = 167$ .

**V. SIMULATION VERIFICATION OF VSG PRE-SYNCHRONIZATION CONTROL**

The simulation verification of VSG synchronous control is to evaluate the performance and effectiveness of this control strategy under different operating conditions. Through simulation, the operation behavior of VSG in micro-grid systems can be simulated, and the control strategy’s ability to adjust output voltage, frequency, and phase can be verified. The simulation validation parameters are shown in Table 1.

**TABLE 1. Simulation verification parameters.**

Parameter	Numerical value
DC side voltage $U_{dc}$	700V
Filter inductor $L_f$	2mH
Filter capacitor $C_f$	30μF
On-off level $f_s$	10kHz
Moment of inertia $J$	0.1kg^m2
Damping coefficient $D$	5
Active power-frequency drop coefficient $K_\omega$	1000
Given merit $P_{ref}$	20kW
Rated angular frequency $\omega_0$	314rad/s
Reactive power-voltage drop coefficient $K_u$	3.89×10-4
Given reactive power $Q_{ref}$	0Var
Rated voltage amplitude $U_0$	311V

The simulation working condition is set to be 23kW in VSG off-grid mode during the 0-0.4 second phase, and the rated active power of VSG is 20kW. According to the operating characteristics of VSG, the output frequency of VSG will be affected by primary frequency modulation and adjusted to approximately 49.8Hz. However, the grid side frequency is rated at 50Hz, resulting in a negative difference between the angular frequency on the output side and that on the grid side. This difference increases gradually over time. This leads to a gradual increase in the phase difference  $\Delta\theta$  between the output side and the power grid side, thereby causing an increase in the voltage difference between the two sides. At 0.4 seconds, a grid connection signal is issued to begin

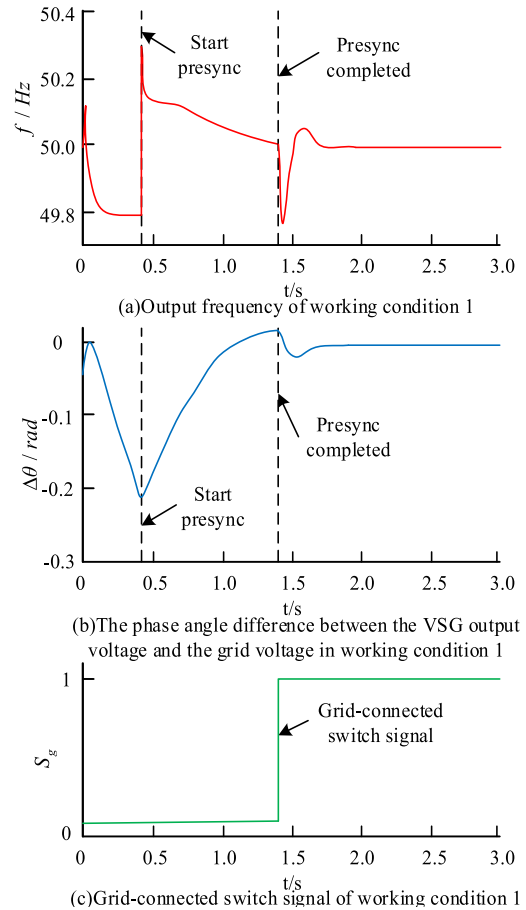


**FIGURE 6. Output frequency and phase angle difference of working condition 1.**

pre synchronization. According to the method of obtaining phase difference information without using a PLL, the phase difference  $\Delta\theta$  between the VSG output side and the grid side voltage can be obtained [29].  $\Delta\theta$  is adjusted by the phase synchronization controller  $H_\theta(s)$ , and the Angular frequency compensation  $\Delta\omega_p$  is added to the output frequency of the VSG active loop to achieve the synchronization of frequency and phase angle. The output frequency and phase angle difference of condition 1 are shown in Figure 6.

In Figure 6 (a), the output frequency stabilizes at 49.8Hz during the time period from 0 to 0.4 seconds. Subsequently, to perform grid connection pre synchronization operation at 0.4 seconds and gradually adjust the output frequency to slowly increase to 50Hz. Figure 6 (b) shows the phase difference  $\Delta\theta$  between the VSG output side and the grid side voltage. During the period of 0 to 0.4 seconds,  $\Delta\theta$  continues to show a negative increasing trend. As the 0.4 second grid connection pre synchronization operation starts,  $\Delta\theta$  gradually decreases. When the time of 1.4 seconds is reached, both the frequency and phase difference are synchronized, and the grid connection switch is turned on, as shown in Figure 6 (c). After about 1.4 seconds, the gateway is successfully set to 1 and switches from off-grid mode to grid connection mode.

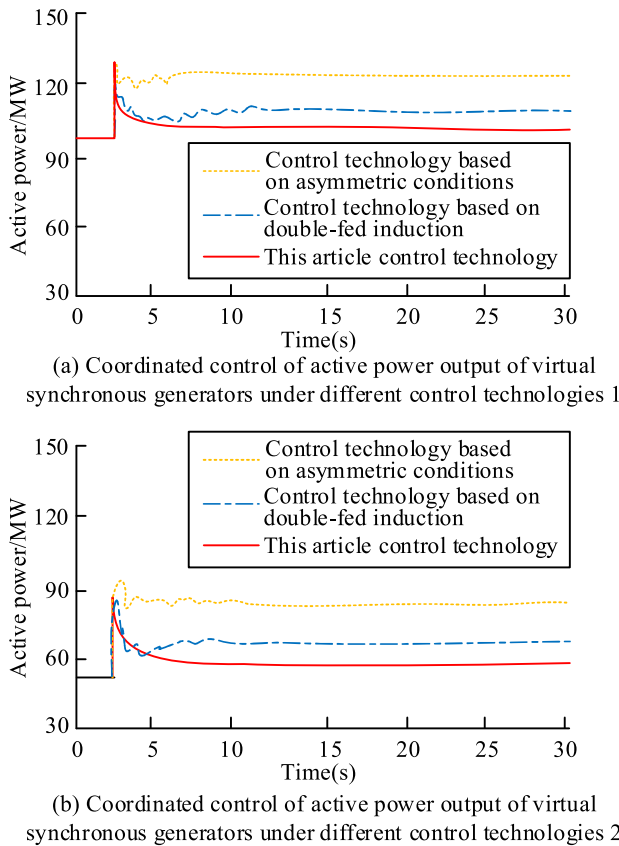


FIGURE 7. Load response and control effect in system simulation model.

The load response and control effect in the system simulation model are shown in Figure 7.

In Figure 7, the simulation model of the system sustains a standard load in the beginning stage (0~2 seconds). Afterwards, a swift increase in load occurs at 2 seconds, with active load surging by 30% within the model. To address this situation, VSG frequency coordination control technology, control technology based on asymmetric conditions, and control technology based on doubly-fed induction are employed. The figure clearly presents the active power output of the VSGs. After the load surge, VSG 1 and generator 2 exhibit power fluctuations. However, the designed control technologies effectively mitigate these fluctuations, reduce the power deficit that arises during load surges, and transfer it into the grid model. The comparison waveform between VSG output voltage and grid voltage under condition 1 is Figure 8.

Figure 8 shows the local comparison waveform between the output voltage of VSG and the grid voltage during the time period of 0.4 seconds to 0.6 seconds. During this period, they shows a gradual trend towards consistency. This implies that the phase difference between the voltage on both sides is gradually decreasing, approaching 0, and the voltage difference is also gradually decreasing. At this point,  $\Delta\theta$  is a negative value, which means that the output voltage of VSG lags behind the grid side voltage. This process clearly indicates that under the pre-synchronization control, the output

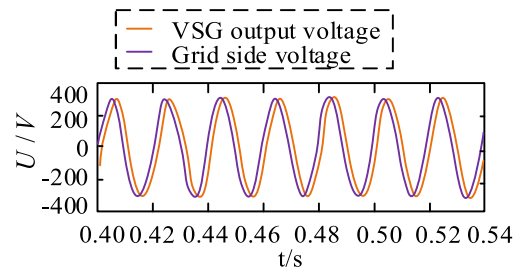


FIGURE 8. Comparison waveform of VSG output voltage and grid voltage in working condition 1.

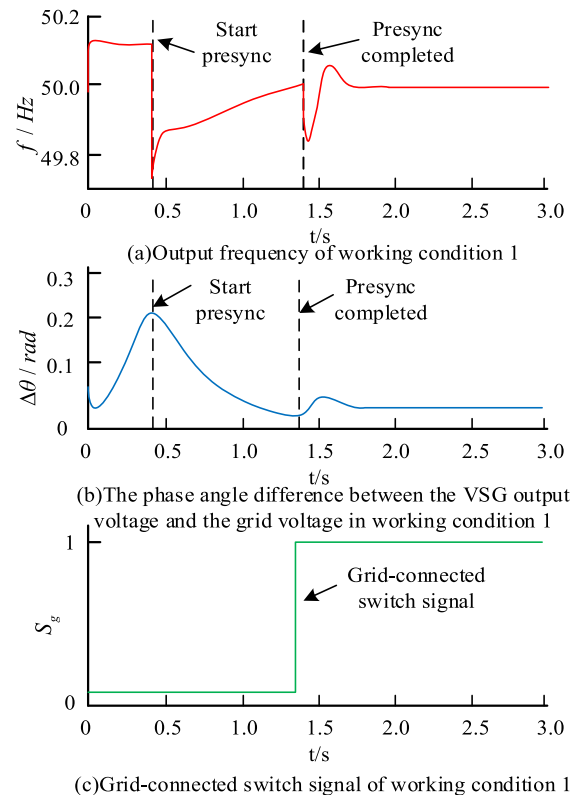


FIGURE 9. Output frequency and phase angle difference of working condition 2.

voltage of VSG gradually synchronizes with the grid voltage, effectively achieving phase and frequency consistency. At the same time, in condition 2, Figure 9 shows the changes in output frequency and phase angle difference, further confirming the effectiveness of the VSG pre-synchronization strategy.

In Figure 9, the following situations can be observed. In the 0-0.4 second stage, the load size of VSG is 17kW, slightly lower than its rated active power of 20kW. Due to the deviation in load size, the output frequency of VSG is 50.2Hz, slightly higher than the rated frequency of the power grid at 50Hz. However, at 0.4 seconds, the grid connection pre synchronization operation is initiated. Through the control strategy, the output frequency of VSG begins to slowly adjust, gradually approaching the rated frequency of 50Hz in the power grid. Figure 9 (c) shows the grid connection



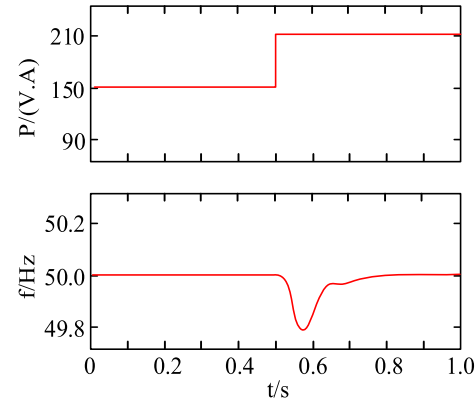
switch signal. At 1.4 seconds, i.e. switching from off-grid mode to grid-connected mode, it can be observed that the grid connected switch signal is set to 1, indicating that the switch from off-grid to grid-connected has been successfully achieved. The experimental micro-grid system parameters are shown in Table 2.

TABLE 2. Experimental micro-grid system parameters.

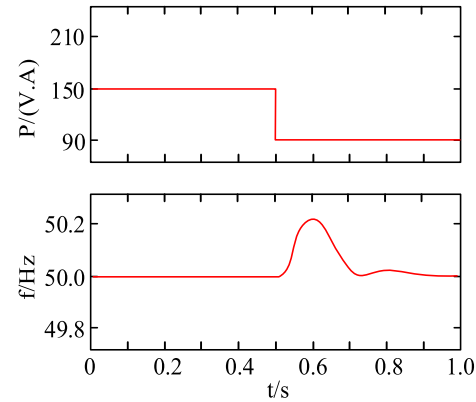
Parameter	Numerical value	Parameter	Numerical value
Rated active power $P_N / (kV \cdot A)$	150	Virtual damping $D / (N \cdot s \cdot m^{-2})$	1
Rated voltage $V_N / V$	30	Virtual inertia $J / (kg \cdot m^2)$	0.1
Rated frequency $f_N / Hz$	50	Droop coefficient $k_f$	-0.0002

As shown in Table 2, to validate the proposed secondary frequency control algorithm based on VSG, the study established a low-voltage testing platform. The system parameters of this platform included the utilization of a PI controller with a proportional factor of 0.5 and an integral factor of 30. The inverter control algorithm was executed within a DSP TMS320F2812. The experiment was conducted in a real-world environment, encompassing two modes: sudden load increase and sudden load decrease. During the experimental process, the system initially operated in a stable rated state and subsequently introduced a load increase or decrease of 60 V·A within 0.5 seconds. The experiments were concluded at 1.0 second.

As shown in Figure 10, compared to the simulation results, there is a slight increase in frequency fluctuations in the actual system. This is due to the slight variation in the system’s operating frequency compared to the simulation. Furthermore, under the same sudden load change conditions, the frequency characteristics of load shedding and load addition are not identical. Specifically, in Figure 10 (a), the frequency decreases rapidly after a load drop, but the frequency recovery is relatively slow after applying the secondary frequency control algorithm. In contrast, in Figure 10 (b), after a load reduction, the frequency rises slowly, but the recovery speed is faster. When the system reaches a stable state, the frequency stability shown in Figure 10(a) exceeds that of Figure 10(b). This is due to differences in the loads. Overall, the experimental results emphasize that the proposed secondary frequency control scheme based on VSG can still maintain the micro-grid frequency within its rated state when dealing with sudden load changes, ensuring the system operates within a safe working range. Overall, the experimental



(a) Operating characteristics of microgrid with sudden load



(b) Operating characteristics of microgrid with sudden load drop

FIGURE 10. Micro-grid load response characteristics.

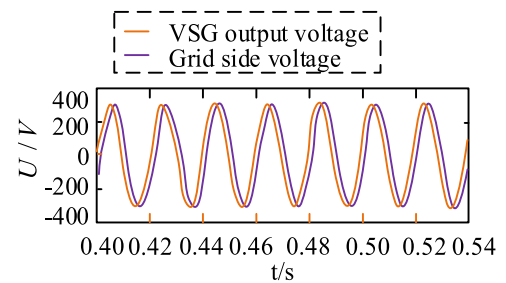


FIGURE 11. Comparison waveform of VSG output voltage and grid voltage in working condition 2.

results highlight that the secondary frequency control scheme based on virtual synchronous generators (VSG) can still maintain the micro-grid frequency within the rated state when dealing with sudden load changes, ensuring that the system operates within a safe operating range. These experimental results verify the validity of the computational simulation results and show that the proposed quadratic frequency control scheme can successfully maintain the frequency stability of the system in a real environment.

As Figure 11, as pre-synchronization progresses, the waveform of VSG output voltage and grid voltage gradually tends to coincide, i.e. the phase difference  $\Delta\theta$  gradually decreases to 0. This means that the phase difference between the VSG

output voltage and the grid voltage is decreasing, and the phases of the two are gradually synchronized. At this point, due to the positive value of  $\Delta\theta$ , the output voltage of VSG is ahead of the grid voltage. This can be concluded by observing the phase difference and voltage difference in the voltage waveform. Meanwhile, as the phase difference  $\Delta\theta$  decreases, the voltage difference also continuously decreases. This indicates that during the pre synchronization, the difference between the VSG output voltage and the grid voltage gradually disappears and eventually becomes consistent.

**VI. EXPERIMENTAL ANALYSIS OF VSG SECONDARY FREQUENCY MODULATION TECHNOLOGY**

According to different integration coefficients, different situations of damping ratio  $\xi$  can be compared. A larger  $\xi$  value means that the frequency recovery process decays faster and there are fewer frequency oscillations, while a smaller  $\xi$  value may lead to longer frequency oscillations and slower frequency recovery. Table 3 shows the different integration coefficients and corresponding damping ratios.

**TABLE 3. Different integral coefficients and corresponding damping ratios.**

Damping ratio $\xi$	Integral coefficient $K_i$
0.17	3000
0.707	167
1.18	60

According to the different integration coefficient values provided in Table 3, the gain of different frequency recovery compensation links is set. Using the same simulation parameters as Table 1, the simulation condition is set to load 20kW within 0-0.2 seconds, and then suddenly to increase the load by 5kW to 25kW at 0.2 seconds. Such sudden load changes will cause frequency changes. The output frequency recovery process of the generator is observed, as shown in Figure 12.

According to the simulation results in Figure 12, the secondary frequency modulation process is divided into two stages: Stage 1 and Stage 2. In stage 1, as the value of  $K_i$  increases,  $t_{s1}$  (duration of stage 1) decreases, and  $\Delta d$  (the absolute value of the difference between the first time  $df/dt$  equals 0 and the rated frequency) also decreases. This is because the increased  $K_i$  leads to strong feedback loop compensation, quickly reducing frequency deviation, thereby shortening the time for frequency recovery to enter stage 2 and reducing frequency oscillation, making frequency recovery more stable. Therefore,  $t_{s1}$  is inversely proportional to  $K_i$ , while  $\Delta d$  is inversely proportional to  $K_i$ . In stage 2, the response characteristics correspond to those of a typical second-order system, where the value of  $K_i$  is inversely proportional to the damping ratio  $\xi$ . The performance of the frequency recovery process is affected by the parameter  $K_i$ . By optimizing the  $K_i$ , a faster and more stable frequency recovery process can be achieved, ensuring stable operation

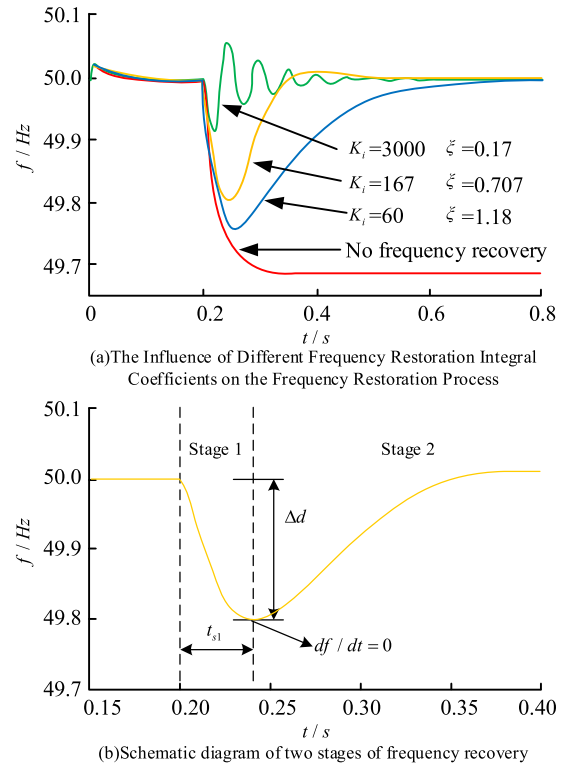


**FIGURE 12. Schematic diagram of the frequency recovery process and its two stages.**

of the power system after sudden load changes. The improved secondary frequency modulation process of the marginal analysis book is observed, as shown in Figure 13.

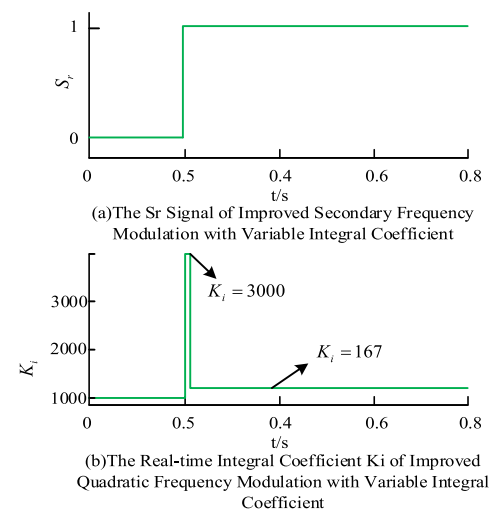


**FIGURE 13. Improved quadratic frequency modulation diagram with variable integral coefficient.**

Figure 13(a) shows that by adopting an improved quadratic frequency modulation strategy with variable integral coefficients, the real-time value of signal  $S_r$  during frequency recovery is consistent with the previous analysis. From Figure 13(b), in frequency recovery stage 1, the value of

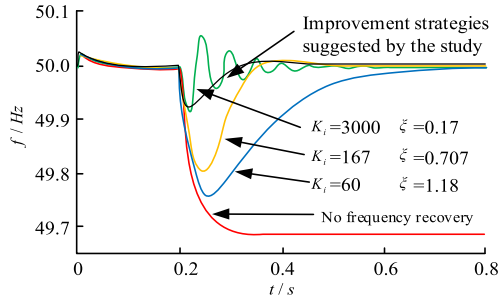


FIGURE 14. Comparison of frequency recovery process between improved strategy and conventional strategy.

real-time integration coefficient  $K_i$  briefly remains at 3000. When entering frequency recovery stage 2, the value of real-time integration coefficient  $K_i$  becomes 167. Under the same simulation conditions as Figure 10, the load size is calculated to be 20kW within the time period of 0-0.2 seconds, and  $\Delta P = 0$  is obtained. At the same time,  $S_r = 0$  indicates that frequency modulation is not performed. At 0.2 seconds, the load suddenly increased by 5kW, reaching 25kW. At this point, it has been calculated that  $P = 5000$  exceeds the safe limit of 3320. This denotes that the size of the load has caused the VSG's output frequency to drop below the permitted range for safe operation. Therefore, at this point, the secondary frequency regulation control strategy is activated,  $S_r = 1$ , which means conducting secondary frequency regulation to restore the frequency of the power system to the specified range.

Figure 14 compares the improved secondary frequency modulation strategy with variable integral coefficient proposed in the study with the conventional fixed integral coefficient secondary frequency modulation strategy. The results show that the strategy proposed in the study has advantages in frequency recovery compared to the conventional fixed integration coefficient strategy: in stage 1, smaller  $t_{s1}$  (duration of stage 1) and  $\Delta d$  are obtained. This means that a larger integration coefficient  $K_i$  is adopted in stage 1, resulting in faster frequency recovery. In stage 2, faster recovery time is achieved and oscillation and other issues are avoided. This indicates that a smaller integration coefficient  $K_p$  is adopted in stage 2 to maintain the stability of frequency recovery and prevent excessive frequency deviation.

In Figure 15, during the 0-0.5 second period, the load was 20kW, and at this time,  $\Delta C$  and  $\Delta P$  were both 0, indicating that the load power was the rated power without frequency deviation. Therefore, the output frequency of VSG was the rated frequency of 50Hz, and the frequency recovery had not started at this time, so  $S_r$  was 0, and the integration coefficient  $K_i$  was taken as 0. At 0.5 seconds, the load suddenly increased by 1kW to 21kW, which meant the load was 21kW between 0.5 seconds and 1 second. At this point,  $\Delta C$  was still 0, but  $\Delta P$  was 1000, indicating a certain frequency deviation due to changes in load. However,  $\Delta P$  was still smaller than  $\Delta P_0$ , so the secondary frequency modulation strategy

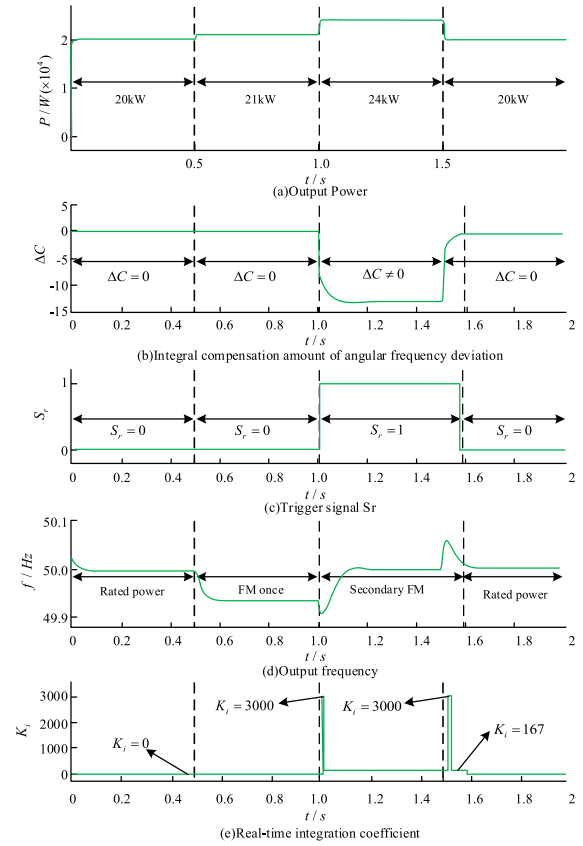


FIGURE 15. The simulation result graph when the load changes continuously.

had not been activated yet. Continue performing primary frequency modulation while affected by virtual inertia, and adjusted the output frequency to 49.94Hz. During this period,  $S_r$  remained at 0 and the secondary frequency modulation strategy was not activated, so  $K_i$  remained at 0. At the moment of 1 second, the load suddenly increased by 3kW again to 24kW, meaning that the load was 24kW during the period of 1 second to 1.5 seconds. At this point,  $\Delta C$  was still 0, but  $\Delta P$  was 4000, exceeding  $\Delta P_0$ . At this point, the secondary frequency modulation strategy was activated and  $S_r$  became 1. Different integration coefficients  $K_i$  were used in frequency recovery stages 1 and 2. In stage 1, the value of  $K_i$  was 3000, which accelerated the frequency recovery speed with a larger  $K_i$ . In stage 2, the value of  $K_i$  was changed to 167 to ensure the stability of frequency recovery. At 1.5 seconds, the load suddenly decreased by 4kW to 20kW, which meant the load was 20kW between 1.5 seconds and 2 seconds. During this period, due to  $\Delta C$  not being equal to 0 and  $S_r$  still being 1, a secondary frequency modulation was performed to adjust the output frequency to 50Hz. After 1.6 seconds,  $\Delta C$  returned to 0 and  $\Delta P$  was also 0, indicating that the load power returned to the rated power. At this point,  $S_r$  returned to 0 and no longer performed frequency modulation. The output frequency remained at the rated frequency of 50Hz.

## VII. CONCLUSION

The research background of VSG pre-synchronization control strategy originates from the demand for the continuous development and improvement of micro-grid systems. This method calculated virtual power by collecting VSG output voltage and grid-side voltage, enabling the calculation of phase angle differences on both sides for pre-synchronization, reducing dependence on PLL. Furthermore, the paper investigated the process of VSG transitioning from grid-connected to off-grid operation and concluded that smooth switching could be achieved by directly disconnecting the grid-connected switch. To address issues with traditional secondary frequency modulation, which employs a fixed integration coefficient for a single VSG, a proposed solution was to use a variable integration coefficient strategy for secondary frequency modulation. The simulation results demonstrated the success of the proposed secondary frequency control scheme based on VSG, gradually adjusting the system frequency from 49.8Hz to 50Hz while maintaining phase synchronization. The study effectively reduced active power fluctuations in VSG 1 and 2 under load transients, enhancing system stability. Furthermore, the paper achieved phase synchronization between VSG output voltage and grid voltage, gradually reducing the phase difference to zero through pre-synchronization. The second stage's performance depended on the damping ratio, with smaller  $K_i$  values contributing to maintaining stability and preventing frequency oscillations. In conclusion, the study introduced a pre-synchronization method that eliminated the need for a PLL, reduced dependence on PLL, and achieved smooth transitions between grid-connected and off-grid modes. Additionally, a variable integral coefficient secondary frequency modulation strategy was proposed to provide faster and more stable frequency recovery capabilities for virtual synchronous power generation systems. In conclusion, this study has introduced a groundbreaking pre-synchronization method that eliminates the need for phase-locked loops, reducing dependence on traditional techniques and achieving smooth transitions between grid-connected and off-grid modes. Furthermore, the proposed variable integral coefficient secondary frequency modulation strategy offers faster and more stable frequency recovery capabilities for virtual synchronous power generation systems. As study move forward, the next phase of research may involve exploring control strategies for other operational states and fault scenarios, further enhancing the applicability of VSG systems and micro-grid technology in practical settings.

## REFERENCES

- [1] A. Muhtadi, D. Pandit, N. Nguyen, and J. Mitra, "Distributed energy resources based microgrid: Review of architecture, control, and reliability," *IEEE Trans. Ind. Appl.*, vol. 57, no. 3, pp. 2223–2235, May 2021.
- [2] X. Zhou, S. Cheng, X. Wu, and X. Rao, "Influence of photovoltaic power plants based on VSG technology on low frequency oscillation of multi-machine power systems," *IEEE Trans. Power Del.*, vol. 37, no. 6, pp. 5376–5384, Dec. 2022.
- [3] X. Chen, Y. Zhang, J. Dong, X. Mao, J. Chen, B. Wen, and Z. Zhang, "A novel pre-synchronization control for grid connection of virtual synchronous generator," *Elektronika Ir Elektrotehnika*, vol. 26, no. 6, pp. 25–31, Dec. 2020.
- [4] V. L. Srinivas, B. Singh, and S. Mishra, "Seamless mode transition technique for virtual synchronous generators and method thereof," *IEEE Trans. Ind. Informat.*, vol. 16, no. 8, pp. 5254–5266, Aug. 2020.
- [5] M. Naderi, Y. Khayat, Q. Shafiee, F. Blaabjerg, and H. Bevrani, "Dynamic modeling, stability analysis and control of interconnected microgrids: A review," *Appl. Energy*, vol. 334, pp. 120647–120668, Mar. 2023.
- [6] K. Shi, W. Song, H. Ge, P. Xu, Y. Yang, and F. Blaabjerg, "Transient analysis of microgrids with parallel synchronous generators and virtual synchronous generators," *IEEE Trans. Energy Convers.*, vol. 35, no. 1, pp. 95–105, Mar. 2020.
- [7] T. Liu, P. Wang, J. Ma, R. Zhang, S. Wang, Z. Wu, and R. Wang, "Presynchronization control for grid-connected inverters without grid voltage sensors," *IEEE Trans. Power Electron.*, vol. 38, no. 3, pp. 2833–2838, Mar. 2023.
- [8] Y. Peng, H. Li, X. Li, J. Wang, and X. Zhang, "Research on pre-synchronization control strategy of optical storage VSG off-grid switching," *Rev. Comput. Eng. Stud.*, vol. 9, no. 1, pp. 23–30, Mar. 2022.
- [9] M. H. Othman, H. Mokhlis, M. Mubin, S. Talpur, N. F. Ab Aziz, M. Dradi, and H. Mohamad, "Progress in control and coordination of energy storage system-based VSG: A review," *IET Renew. Power Gener.*, vol. 14, no. 2, pp. 177–187, Feb. 2020.
- [10] B. Qin, Y. Xu, C. Yuan, and J. Jia, "A unified method of frequency oscillation characteristic analysis for multi-VSG grid-connected system," *IEEE Trans. Power Del.*, vol. 37, no. 1, pp. 279–289, Feb. 2022.
- [11] Y. Liu, Y. Wang, M. Wang, Z. Xu, Y. Peng, and M. Li, "Coordinated VSG control of photovoltaic/battery system for maximum power output and grid supporting," *IEEE J. Emerg. Sel. Topics Circuits Syst.*, vol. 12, no. 1, pp. 301–309, Mar. 2022.
- [12] D. Melcher, M. Bätge, and S. Neßlinger, "A novel rotor blade fatigue test setup with elliptical biaxial resonant excitation," *Wind Energy Sci.*, vol. 5, no. 2, pp. 675–684, May 2020.
- [13] J. Liu, J. Li, H. Song, A. Nawaz, and Y. Qu, "Nonlinear secondary voltage control of islanded microgrid via distributed consistency," *IEEE Trans. Energy Convers.*, vol. 35, no. 4, pp. 1964–1972, Dec. 2020.
- [14] L. Zhou, S. Liu, Y. Chen, W. Yi, S. Wang, X. Zhou, W. Wu, J. Zhou, C. Xiao, and A. Liu, "Harmonic current and inrush fault current coordinated suppression method for VSG under non-ideal grid condition," *IEEE Trans. Power Electron.*, vol. 36, no. 1, pp. 1030–1042, Jan. 2021.
- [15] M. Zarif Mansour, S. P. Me, S. Hadavi, B. Badrzadeh, A. Karimi, and B. Bahrani, "Nonlinear transient stability analysis of phased-locked loop-based grid-following voltage-source converters using Lyapunov's direct method," *IEEE J. Emerg. Sel. Topics Power Electron.*, vol. 10, no. 3, pp. 2699–2709, Jun. 2022.
- [16] X. Yan, C. Wang, Z. Wang, H. Ma, B. Liang, and X. Wei, "A united control strategy of photovoltaic-battery energy storage system based on voltage-frequency controlled VSG," *Electronics*, vol. 10, no. 17, p. 2047, Aug. 2021.
- [17] S. Chen, Y. Sun, H. Han, S. Fu, S. Luo, and G. Shi, "A modified VSG control scheme with virtual resistance to enhance both small-signal stability and transient synchronization stability," *IEEE Trans. Power Electron.*, vol. 38, no. 5, pp. 6005–6014, May 2023.
- [18] C. Li, Y. Yang, N. Mijatovic, and T. Dragicevic, "Frequency stability assessment of grid-forming VSG in framework of MPME with feedforward decoupling control strategy," *IEEE Trans. Ind. Electron.*, vol. 69, no. 7, pp. 6903–6913, Jul. 2022.
- [19] X. Hou, Y. Sun, X. Zhang, J. Lu, P. Wang, and J. M. Guerrero, "Improvement of frequency regulation in VSG-based AC microgrid via adaptive virtual inertia," *IEEE Trans. Power Electron.*, vol. 35, no. 2, pp. 1589–1602, Feb. 2020.
- [20] J. Chen, X. Yang, T. Zhao, and P. Li, "Simulation analysis and verification of take-up judder caused by cumulative geometric deviation of clutch friction plates," *Vibroeng. Proc.*, vol. 42, pp. 64–69, May 2022.
- [21] C. Liu, X. Wang, Y. Ren, X. Wang, and J. Zhang, "A novel distributed secondary control of heterogeneous virtual synchronous generators via event-triggered communication," *IEEE Trans. Smart Grid*, vol. 13, no. 6, pp. 4174–4189, Nov. 2022.
- [22] J. Li, B. Wen, and H. Wang, "Adaptive virtual inertia control strategy of VSG for micro-grid based on improved bang-bang control strategy," *IEEE Access*, vol. 7, pp. 39509–39514, 2019.



- [23] S. Lu, T. Wang, Y. Liang, S. Cheng, Y. Cai, H. Wang, J. Yang, Y. Sui, and L. Yang, "Low-frequency oscillation analysis of grid-connected VSG system considering multi-parameter coupling," *Comput. Model. Eng. Sci.*, vol. 135, no. 3, pp. 2373–2386, 2023.
- [24] S. Fu, Y. Sun, L. Li, Z. Liu, H. Han, and M. Su, "Power oscillation suppression in multi-VSG grid by adaptive virtual impedance control," *IEEE Syst. J.*, vol. 16, no. 3, pp. 4744–4755, Sep. 2022.
- [25] Y. Xu, R. Viswanatha, O. Sitsel, D. Roderer, H. Zhao, C. Ashwood, C. Voelcker, S. Tian, S. Raunser, N. Perrimon, and M. Dong, "CRISPR screens in *Drosophila* cells identify VSG as a TC toxin receptor," *Nature*, vol. 610, no. 7931, pp. 349–355, Oct. 2022.
- [26] W. Chen, B. Liu, M. S. Nazir, A. N. Abdalla, M. A. Mohamed, Z. Ding, M. S. Bhutta, and M. Gul, "An energy storage assessment: Using frequency modulation approach to capture optimal coordination," *Sustainability*, vol. 14, no. 14, p. 8510, Jul. 2022.
- [27] Y. Wu, C. Huang, F. Dong, G. Li, G. Wang, and S. Zhang, "Study on frequency stability of an independent system based on wind-photovoltaic-energy storage-diesel generator," *Electronics*, vol. 11, no. 23, p. 3956, Nov. 2022.
- [28] Y. Zhang, Q. Sun, J. Zhou, J. M. Guerrero, R. Wang, and A. Lashab, "Optimal frequency control for virtual synchronous generator based AC microgrids via adaptive dynamic programming," *IEEE Trans. Smart Grid*, vol. 14, no. 1, pp. 4–16, Jan. 2023.
- [29] P. Liu, Y. Bi, and C. Liu, "Data-based intelligent frequency control of VSG via adaptive virtual inertia emulation," *IEEE Syst. J.*, vol. 16, no. 3, pp. 3917–3926, Sep. 2022.



**NURULAZLINA RAMLI** (Member, IEEE) was born in Sri Aman, Sarawak, Malaysia, in 1984. She received the B.Eng. degree in electrical engineering (telecommunication) from Universiti Teknologi Malaysia (UTM), Malaysia, in 2008, and the M.Sc. degree in telecommunication and information engineering and the Ph.D. degree in electrical engineering from Universiti Teknologi Mara (UiTM), Shah Alam, Selangor, Malaysia, in 2011 and 2015, respectively.

She has been a Lecturer with the Faculty of Engineering, Built Environment, and Information Technology (FoEBEIT), SEGi University, Malaysia, since September 2015, where she became the Research Cluster Head for Engineering and Technology, in January 2023, and continues to hold this position. Additionally, she was appointed as a member of the SEGi Research Ethics Committee in the Engineering and Technology Cluster, from January 2023 to December 2023. Furthermore, she has been the Head of the Centre for Advanced Electrical and Electronic Systems (CAEES), SEGi University, since 2018. In addition to her responsibilities at SEGi University, she was appointed as a Fellow Researcher [Ahli Bersekutu Kumpulan Penyelidik (RG)] with the Antenna Research Centre, School of Electrical Engineering, College of Engineering, UiTM, from April 2022 to March 2024. Since 2018, she has actively participated as a Judge in local and international competitions, particularly events organized by the Indonesian Young Scientist Association (IYSA). Between July 2008 and December 2009, she was a Postgraduate Assistant (Tutor) with the Faculty of Electrical Engineering, Universiti Teknologi Petronas (UTP), Sri Iskandar, Perak, Malaysia. She has been appointed as a Research Fellow with the Antenna Research Centre (ARC), UiTM, and she has been a Group Leader of the Centre for Advanced Electrical Electronics System (CAEES), SEGi University, since 2018. She is also a Graduate Member of the Institution of Engineers Malaysia (IEM) and a registered member of the International Association of Engineers (IAENG). She supervises many Ph.D./M.Sc. students and she has authored several journal articles and conference papers. Her research interests include the areas of radio frequency and microwave (antenna design), computational intelligence, wireless communication, 5G, the IoT, and electronics communications.

Dr. Ramli received the Best Paper Award, in 2012, at the IEEE Asia Pacific Conference on Applied Electromagnetics (APACE) for her novelty and contributions to her research.



**NOOR HAFIZAH ABDUL AZIZ** received the Bachelor of Engineering degree majoring in microelectronic engineering and the Master of Science degree in electrical, electronic, and system engineering from Universiti Kebangsaan Malaysia (UKM), Malaysia, in 2004 and 2007, respectively, and the Ph.D. degree majoring in wireless communications engineering from Universiti Putra Malaysia (UPM), in 2018. She is currently a Lecturer with the School of Electrical Engineering, College of Engineering, Universiti Teknologi MARA, (UiTM), Malaysia. Her research interest includes passive forward scattering radar applications.

• • •



**JIANFENG WANG** was born in Tonghua, Jilin, China, in 1980. He received the bachelor's degree in electrical engineering and automation from China Agricultural University, in 2003, and the master's degree in communication and information systems from North China Electric Power University, in 2007. He is currently pursuing the Ph.D. degree in engineering with SGEI University.

From 2007 to 2023, he was a Lecturer with the Department of Information Engineering, North China Electric Power University Science and Technology College. Since 2023, he has been an Associate Professor with the Faculty of Electrical Engineering, Hebei Vocational University of Technology and Engineering. Since 2007, he has been published a total of 17 research articles, including four articles indexed in Web of Science (WOS) and three articles indexed in Engineering Index (EI). He has authored one academic monograph, obtained two utility model patents, and secured four software copyrights. Additionally, he has led and participated in a total of 15 research projects.